Stochastic hybrid modeling of intracellular calcium dynamics

TaiJung Choi,[1,a)] Mano Ram Maurya,[2,b)] Daniel M. Tartakovsky,[1,c),d)] and Shankar Subramaniam[2,3,c),e)]

[1]*Department of Mechanical and Aerospace Engineering, University of California, San Diego, La Jolla, California 92093, USA*
[2]*Department of Bioengineering, University of California, San Diego, La Jolla, California 92093, USA*
[3]*Department of Cellular and Molecular Medicine, Department of Chemistry and Biochemistry, and Graduate Program in Bioinformatics, University of California, San Diego, La Jolla, California 92093, USA*

Deterministic models of biochemical processes at the subcellular level might become inadequate when a cascade of chemical reactions is induced by a few molecules. Inherent randomness of such phenomena calls for the use of stochastic simulations. However, being computationally intensive, such simulations become infeasible for large and complex reaction networks. To improve their computational efficiency in handling these networks, we present a hybrid approach, in which slow reactions and fluxes are handled through exact stochastic simulation and their fast counterparts are treated partially deterministically through chemical Langevin equation. The classification of reactions as fast or slow is accompanied by the assumption that in the time-scale of fast reactions, slow reactions do not occur and hence do not affect the probability of the state. Our new approach also handles reactions with complex rate expressions such as Michaelis–Menten kinetics. Fluxes which cannot be modeled explicitly through reactions, such as flux of Ca^{2+} from endoplasmic reticulum to the cytosol through inositol 1,4,5-trisphosphate receptor channels, are handled deterministically. The proposed hybrid algorithm is used to model the regulation of the dynamics of cytosolic calcium ions in mouse macrophage RAW 264.7 cells. At relatively large number of molecules, the response characteristics obtained with the stochastic and deterministic simulations coincide, which validates our approach in the limit of large numbers. At low doses, the response characteristics of some key chemical species, such as levels of cytosolic calcium, predicted with stochastic simulations, differ quantitatively from their deterministic counterparts. These observations are ubiquitous throughout dose response, sensitivity, and gene-knockdown response analyses. While the relative differences between the peak-heights of the cytosolic $[Ca^{2+}]$ time-courses obtained from stochastic (mean of 16 realizations) and deterministic simulations are merely 1%–4% for most perturbations, it is specially sensitive to levels of $G_{\beta\gamma}$ (relative difference as large as 90% at very low $G_{\beta\gamma}$). © *2010 American Institute of Physics.* [doi:10.1063/1.3496996]

I. INTRODUCTION

Intracellular signaling is an important event in cellular life that mediates most of its functions, such as adaptation in response to environmental changes and regular functions including metabolism, cellular growth, and proliferation. Mathematical modeling has helped to explain and illustrate many of these complex phenomena, including the bistability and graded versus switchlike response in intracellular signaling,[1] autocatalysis as a mechanism of positive feedback in the cell cycle,[2] and subpopulation variability.[3] Much of this modeling is done in a deterministic setting and involves systems of coupled ordinary differential equations (ODEs) describing the rate of change of components (reactants and products) of the biochemical reactions and other processes involved in the pathway.

ODE-based formulations provide accurate predictions of the dynamics of biochemical pathways with large numbers of molecules of all reacting species, but might fail when the concentrations of reactants and/or products become exceedingly small so that only a few molecules (less than ten in some cases) are involved.[4] Indeed, for small volumes and small concentrations that often characterize subcellular processes, the very concept of concentration breaks down. When this occurs, randomness associated with the dynamics of individual molecules becomes pronounced, necessitating the use of probabilistic (stochastic) models. A chemical master equation (CME) yields an exact probabilistic description of multispecies reactions, but its high dimensionality renders it computationally prohibitive.

Gillespie's stochastic simulation algorithm[5] (SSA) provides an exact sampling of the solution of the CME, thus providing highly accurate results with sufficient sampling. The computational efficiency of the SSA can be increased by adopting, for example, a tau-leap algorithm[6] or its continuous-limit approximation in the form of a chemical Langevin equation (CLE).[7] Implicit in these and other ap-

proximations of the SSA is a trade-off between computational speed-up and accuracy, which undermines their use in complex multiscale biochemical phenomena involving fast and slow reactions. A quasi-steady-state approximation,[8] which neglects the fast reactions by assuming that a subset of chemical species is at steady state at the timescale of interest, is efficient but clearly inexact.

Some of the more recent contributions in this area include (1) speed-up of computation through a binomial tau-leaping approach[9] and k-skip method,[10] (2) time-scale/reaction partitioning based on the propensity values,[11] a hybrid approach,[12] and quasi-steady-state approximation,[13] (3) partial-propensity-based approach,[14] and (4) alternative formulations of CLE.[15] Besides, Cai[16] has developed an approach to perform stochastic simulation of reaction systems with time-delays. Frazier *et al.*[17] have developed a software called BIOMOLECULAR NETWORK SIMULATOR to study various aspects of stochastic simulation of complex biomolecular reaction networks. Gillespie *et al.*[18] have presented a detailed analysis of issues in simplification of Michaelis–Menten formulation into a single-step reaction in stochastic simulation. Rathinam *et al.*[19] have developed a methodology for parametric sensitivity analysis in stochastic simulation of reaction networks. By no means this is an exhaustive list.

Hybrid methods, e.g., by Salis and Kaznessis,[12] which we pursue here, address the multiscale nature of reactive systems by identifying fast and slow reactions and simulating the former with a CLE and the latter with Gillespie's SSA. This approach significantly reduces simulation time without compromising the accuracy of the outputs. We present a hybrid algorithm in which slow and fast reactions are identified *a priori*, they can be reclassified during simulation in response to changes in concentrations, and we can deal with complex fluxes that cannot be modeled explicitly through reactions. An example of such a flux, in the model of cytosolic calcium dynamics, is the flux of $[Ca^{2+}]$ from the endoplasmic reticulum to the cytosol through inositol 1,4,5-trisphosphate receptor channels (please see the expression for J_{ch} in Sec. III C 2).

We have used the dynamics of cytosolic calcium as a case study to test our approach. The cytosolic calcium dynamics and its mathematical descriptions are briefly discussed in Sec. II to motivate the development of a multiscale stochastic hybrid algorithm (SHA) in Sec. III, which consists of the following steps. Section III A contains a formulation of the calcium dynamics model used in our analysis. In Sec. III B, we compare the performance of the existing stochastic approaches, i.e., the Gillespie's SSA, a tau-leap algorithm, and a chemical Langevin equation. In Sec. III C, we present the SHA, which consists of deterministic and stochastic components, explicitly accounts for the presence of slow and fast reactions, and incorporates complex fluxes that cannot be modeled through reactions explicitly. An approach to handle reactions with complex rate expressions is also presented in this section explaining why the existing approaches to deal with complex rates laws such as Michaelis–Menten mechanism[8,13,18] may not be directly applicable. The practical implementation of the SHA to the cytosolic calcium dynamics model[3] is presented in Sec. III D. Section IV contains
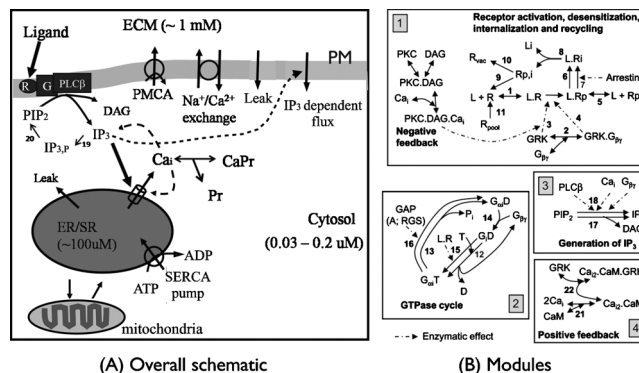

FIG. 1. A simplified model for calcium signaling including calcium influx, ER, and mitochondrial exchange and storage [diagram in panel B taken from Maurya and Subramaniam (Ref. 3) *with permission from Biophysical Journal*]. (a) Ligand Complement 5a (C5a) binds to its receptor on plasma membrane (PM) and activates G protein G_i. The free $G_{\beta\gamma}$ binds to PLCβ and increases its activity which accelerates the phosphorylation of PIP_2 into IP_3 and DAG. IP_3 binds to its receptor IP_3R on the ER membrane. Thus, calcium from the ER is released into the cytosol. Other fluxes between cytosol and mitochondria or ECM are also shown. (b) Receptor module (box 1), GTPase cycle module (box 2), IP_3 generation module (box 3), and feedback module (box 4); ECM, extracellular matrix; PIP_2, phosphatidylinositol 4,5-bisphosphate; IP_3, inositol 1,4,5-trisphosphate; $IP_{3,p}$, a lumped product of IP_3 phosphorylation; Ca_i, cytosolic Ca^{2+}; Pr, proteins; ER, endoplasmic reticulum; ATP, adenosine triphosphate; ADP, adenosine diphosphate; SERCA, sarco(endo) plasmic reticulum calcium ATPase; PMCA, plasma membrane calcium ATPase; NCX, Na^+/Ca^{2+} exchanger; L, ligand C5a; R, receptor C5aR; GRK, G-protein-coupled receptor kinase; CaM, calmodulin; PLCβ, phospholipase C-β; GAP, GTPase activating protein; RGS, regulator of G-protein signaling; DAG, diacylglycerol; PKC, protein kinase C; Pi, phosphate.

the results of stochastic simulations of cytosolic calcium dynamics, whose biological implications are further discussed in Sec. V.

II. DYNAMICS OF CYTOSOLIC CALCIUM

Cytosolic calcium is a second messenger that plays an important role in intracellular signaling. Dynamic changes in intracellular calcium serve both as an important indicator of cellular events and as a quantitative measure of cellular response to stimuli. In addition to affecting gene regulation, calcium regulates the activity of many proteins such as calmodulin,[20] calreticulin,[21–23] and calcineurin.[24] Through such regulation, cytosolic calcium affects many functions including muscle contraction, fertilization, learning and memory, among many others.

A. Biological mechanisms and pathways

Following Maurya and Subramaniam,[3] we consider a signaling network for calcium dynamics (Fig. 1), which represents the ligand-induced release of calcium from the endoplasmic reticulum (ER) into cytosol, binding of calcium (Ca_i) to proteins (Pr) in the cytosol (shown) and in the ER (not shown) and other calcium exchange fluxes to/from the ER, the extracellular space and mitochondria. In the basal state, the channel flux from the ER is very small and, along with the leakage flux from the ER, is balanced by the Ca^{2+} uptake back into the ER by the sarco(endo)plasmic reticulum calcium ATPase (SERCA) pump; the net flux across the mitochondria and the PM is zero; and the Ca^{2+} outflux from the

cytosol to the extracellular matrix (ECM) is mediated by the plasma membrane calcium ATPase (PMCA) pump and the Na$^+$/Ca^{2+} exchanger (NCX). The influx across the plasma membrane consists of a nonspecific leakage flux and an [IP$_3$]-dependent specific flux, which combines many fluxes including the entry through store-operated channels in response to the ER depletion and other effects.[25] Ca^{2+} binds to buffer proteins in all three compartments, the cytosol, the ER, and the mitochondria, for which rapid buffering kinetics suggested earlier[26,27] is used. For a more detailed analysis of the perturbation of the calcium network, we refer the reader to Maurya and Subramaniam.[28]

Maurya and Subramaniam[3] developed a kinetic model for calcium signaling in mouse macrophagelike RAW 264.7 cell and simulated the calcium dynamics for the ligand Complement 5a (C5a). In nonexcitable cells, such as macrophages, ligand-induced release of calcium from the ER is the main initiator of calcium dynamics. Upon stimulation with C5a, the C5a receptor (C5aR) becomes activated leading to activation of G-protein, G$_{\alpha,i}$ followed by activation of phospholipase C (PLC) β (PLCβ). The net result is increased hydrolysis of phosphatidylinositol 4,5-bisphosphate (PIP$_2$) into inositol 1,4,5-trisphosphate (IP$_3$), and increase in the levels of cytosolic calcium ([Ca^{2+}]$_i$) due to the opening of IP$_3$ receptor (IP$_3$R) channels on the endoplasmic (or sarcoplasmic) reticulum (ER/SR) membrane.[29] The concentration of calcium in the cytosol is in submicromolar range, whereas it can be 10–100 s micromolar (μM) in the ER.[29] Hence, upon opening of the IP$_3$R channels, the large gradient of calcium between the ER and the cytosol results in a burst (large peak) of [Ca^{2+}]$_i$ response.[29] Through a positive feedback mechanism, also known as calcium-induced calcium release (CICR),[30,31] more Ca^{2+} is released from the ER into the cytosol. Most of the calcium released binds to various proteins, such as calmodulin (CaM). Calcium is also pumped back to the ER by the SERCA pump. Some calcium is also expelled to the extracelluar space through the Na^{2+}/Ca^{2+} exchanger (NCX) and the PMCA pump. The resulting calcium current facilitates the cross-talk between calcium dynamics and action potential in cardiac pacemaker cells.[32] Calcium exchange between cytosol and mitochondria also has been observed at elevated level of [Ca^{2+}]$_i$.

B. Mathematical representations of calcium dynamics

Mathematical models of cytosolic calcium dynamics were developed for both excitable[33–37] cells and nonexcitable[27,33,38] cells. Many of these models deal with spatial distribution of calcium by employing two- or three-dimensional partial-differential equations.[39] Most of such models rely on nonspecific (independent of cell-type) parameter values and provide qualitative (rather than quantitative) predictions of the behavior of various cell types. Moreover, they fail to capture the calcium dynamics in RAW 264.7 cells without parameter-tuning.[3]

The Maurya and Subramaniam[3] model overcomes these limitations by using experimental measurements in RAW cells to constrain parameter values. The model neglects molecular diffusion, the presence of IP$_3$R clusters, and local-

concentration effects in the mechanism for calcium release from the ER,[40] all of which are accounted for in the work by Greenstein et al.,[35] Jafri et al.,[41] and Puceat and Jaconi.[42] On the other hand, it includes detailed mechanisms of G-protein coupled receptor and G-protein activation and inactivation, which are absent in the works of Hofer et al.,[25] Lemon et al.,[27] Wiesner et al.,[38] and Fink et al.[39] The model enables the analysis of the effects of single and multiple knockdowns of proteins and subpopulational variability, i.e., to account for the fact that different cell-populations, when triggered by the same strength of a stimulus, result in quantitatively and qualitatively different responses (different peak-heights, rise-times, etc.).[43] Hence, we adopt the signaling network identified by Maurya and Subramaniam[3] as the basis for the present analysis. The focus of the modeling studies is on the sensitivity analysis of the peak-height of cytosolic Ca^{2+} to stochastic versus deterministic simulation.

III. MATERIALS AND METHODS

A mathematical representation of the signaling network identified by Maurya and Subramaniam[3] is presented in Sec. III A. The performance of standard stochastic simulation algorithms is compared in Sec. III B. A new hybrid algorithm that significantly improves the computational efficiency of the standard stochastic algorithms is presented in Sec. III C. The application of the hybrid algorithm to the cytosolic calcium dynamics model[3] is presented in Sec. III D.

A. The mathematical model of cytosolic calcium dynamics

A system of ODEs that describe the cytosolic calcium dynamics[3] accounts for the chemical reactions grouped into the four modules in Fig. 1(b). The receptor module (box 1) consists of the reactions 1–11 responsible for receptor activation, desensitization of the ligand-bound active receptor due to its phosphorylation, internalization of the ligand-bound phosphorylated receptor, and receptor recycling. The GTPase cycle module (box 2) consists of reactions 12–16 corresponding to activation and deactivation of G-protein (G-protein is active when G$_{\beta\gamma}$ and G$_{\alpha,i}$T are separated). The IP$_3$ module (box 3) includes activation of PLCβ upon binding of G$_{\beta\gamma}$ and cytosolic Ca^{2+} and subsequently catalyzed hydrolysis of PIP$_2$ into IP$_3$ and DAG. Reactions 19 and 20 capture IP$_3$ metabolism, i.e., its degradation/conversion to/from other inositol-phosphates and back to PIP$_2$, with only one intermediate pseudospecies, namely, IP$_{3,p}$ or IP$_3$ product [Fig. 1(a)].[27] Positive feedback effects from calmodulin constitute the fourth module (box 4).

The cytosol and other compartments are assumed to be well-mixed. The state variables are described by a set of ODEs (Ref. 44) involving the Ca^{2+} fluxes between different cellular compartments and other fluxes due to reactions. The 15 state variables (concentrations) used to model the details of ligand-induced generation of IP$_3$ are [L], [R], [LR], [G$_{\beta\gamma}$], [GRK], [LR$_p$], [R$_p$], [LR$_i$], [R$_{p,i}$], [R$_{pool}$], [G$_{\alpha,i}$T], [G$_{\alpha,i}$D], [PIP$_2$], [IP$_3$], and [CaM]. [X] represents concentration of species X. These differential equations involve fluxes only related to reactions modeled explicitly. Calcium dynamics
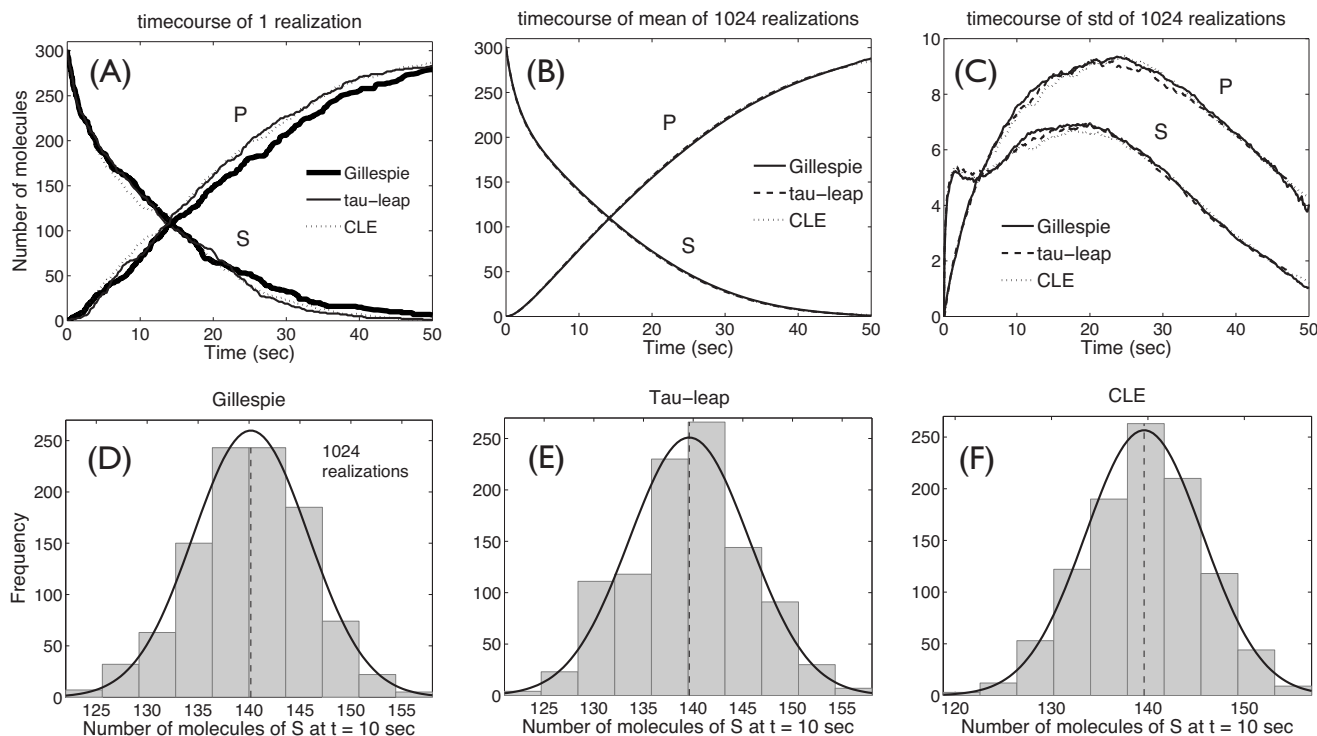
FIG. 2. Temporal evolution of the concentrations of substrate $S(t)$ and product $P(t)$ computed using the Gillespie, tau-leap, and CLE approaches. (a) shows time-course of one realization from each method. (b) and (c) show the time-course of mean and standard deviation from 1024 realizations, which show excellent agreement among the three different methods. (d)–(f) show histograms and probability distribution of the number of molecules of S sampled at t =10 s. The shapes of the three histograms are very similar.

introduces four additional state variables: $[\text{Ca}^{2+}]_i$, $[\text{Ca}^{2+}]_{\text{ER}}$, h and $[\text{Ca}^{2+}]_{\text{mit}}$, where $[\text{Ca}^{2+}]_{\text{ER}}$ and $[\text{Ca}^{2+}]_{\text{mit}}$ denote the concentrations of free Ca^{2+} in the ER and mitochondria, respectively; and h is the fraction of IP_3R to which calcium is not bound at the inhibitory site (IP_3 and calcium may or may not be bound at the other two sites, respectively).[45] These differential equations deal with flux expressions due to complex lumped mechanisms which cannot be modeled through reactions explicitly. Thus, the model by Maurya and Subramaniam[3] has 19 state variables. The quantities of all chemical species are in terms of their concentrations, normalized with respect to a unit volume of the cytosol. The model involves 65 reaction-rate parameters, including both simple and complex reaction fluxes and other flux exchanges between different compartments.

In this analysis, we focus on the calcium dynamics in the regimes with exceedingly small concentrations of relevant chemical compounds. To give an example, for dose response, corresponding to the lowest dose of the ligand C5a, the number of the molecules is 180 (0.1% of 30 nM concentration). In another case, in sensitivity analysis of $G_{\beta\gamma}$, the number of molecules of $G_{\beta\gamma}$ (total pool) considered is 2500 at 5% level of nominal value. Corresponding to this, the number of molecules of free $G_{\beta\gamma}$ is 10. In such regimes, the fidelity of continuum (ODE-based) descriptions might be compromised, and stochastic effects become important.

B. Comparison of computational efficiency of stochastic simulation algorithms

For the sake of completeness, in Appendix, we present a brief overview of the existing stochastic algorithms, namely,

Gillespie algorithm, tau-leap method, and chemical Langevin equation. To compare their performance, we have applied these three algorithms to an enzymatic reaction satisfying the Michaelis–Menten rate law (example taken from Ref. 46),

$$S + E \overset{c_1}{\rightarrow} C, \quad C \overset{c_2}{\rightarrow} S + E, \quad C \overset{c_3}{\rightarrow} P + E, \tag{1}$$
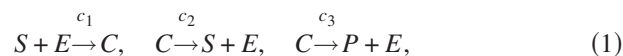
where S, E, C, and P denote the substrate, enzyme, enzyme-substrate complex, and product, respectively, or the number of their molecules. Figure 2 shows the temporal evolution of $S(t)$ and $P(t)$ from their initial levels $S(0)=312$, $E(0)=125$, and $P(0)=0$, computed with the three approaches for stochastic simulation described above. The three algorithms yield similar predictions, with the tau-leap and CLE algorithms giving nearly indistinguishable solutions.

Figure 2(a) shows time-course of one realization from each method. Although the single time-courses show good agreement, time-course of mean and standard deviation of 1024 realizations are computed as well in order to ensure that they have similar statistical characteristics. Figures 2(b) and 2(c) show excellent agreement among three algorithms in terms of mean and standard deviation. Next three histograms show probability distribution of the number of molecules of S sampled at t=10 s [Figs. 2(d)–2(f)]. The three histograms have almost same values of the mean ([Gillespie, Tau-leap, CLE]=[140.40, 139.25, 139.89]) and the standard deviation ([Gillespie, Tau-leap, CLE] =[5.84, 6.09, 6.06]).

Table I demonstrates the scalability of the three stochastic algorithms with the number of molecules involved in the simulation of Eq. (1). As the initial number of molecules,

TABLE I. The run-time scalability of the Gillespie, tau-leap, and chemical Langevin equation algorithms as a function of the number of molecules.

	Initial number of molecules	
	S: 312, E: 125	S: 31 200, E: 12 500
Method	Computation time (second)	Computation time (second)
Gillespie algorithm	0.892	100.3
Tau-leap algorithm	0.235	0.354
CLE	0.003	0.003

$S(0)$ and $P(0)$, increases 100-fold, the computation time of the Gillespie algorithm increases almost 100-fold, while the run times of the tau-leap and CLE algorithms remain practically unchanged. The run times reported represent MATLAB simulations carried out on a Windows based PC with 2.1 GHz Intel dual core processor and 2 GB RAM.

C. A multiscale hybrid approach

While the use of the CLE is appealing due to its computational efficiency, its accuracy suffers as the number of molecules involved in the chemical reactions becomes small. Likewise, the Gillespie algorithm is attractive due to its accuracy but it becomes inefficient when the number of chemical reactions and/or molecules becomes large. This dichotomy calls for the use of a hybrid approach (described in Sec. III C 1 below) in which fast reactions are tackled with the CLE, and the Gillespie algorithm is employed to simulate slow reactions.

An additional complication in modeling the cytosolic calcium dynamics arises from the presence of fluxes in which reactions are either absent or modeled implicitly and, hence, are not readily amenable to the stochastic formulations described above. These fluxes are modeled deterministically via ODEs as described in Sec. III C 2, giving rise to a stochastic-deterministic hybrid approach. Besides, the rate expressions for some reactions are complex. These rate expressions are a combination (function) of one or more law of mass action kinetics, Michaelis–Menten kinetics or Hill-dynamics-based terms. A stochastic treatment of such reactions in terms of propensity functions is described in Sec. III C 3. Our new multiscale hybrid approach accounts for all these three scenarios.

1. Multiscale approach

In many complex biochemical systems, including the cytosolic calcium dynamics, some reactions occur very frequently over short time-intervals, while others seldom occur. In deterministic ODE-based models, the Jacobian matrix, which is a function of both the reaction rate constants and the species concentrations, can be used to classify species as fast or slow. In particle-based stochastic simulations, the system proceeds through firing of reactions and hence the speed of both the reactions and species is important. To call a reaction "slow" or "fast," the knowledge of reaction rate constants alone is not sufficient. Indeed, a reaction with a large reaction rate constant cannot be classified as fast if they involve

small numbers of reactant species. The approach presented below is, essentially, based on the work of Salis and Kaznessis[12] and Haseltine and Rawlings[47] (see also the contribution of Haseltine and Rawlings[48]).

Following Salis and Kaznessis,[12] we classify a jth reaction as fast if the following two constraints on the propensity function [Eq. (A2)] and the number of molecules of each species involved in the reaction are simultaneously satisfied,

$$a_j[\mathbf{X}(t)]dt \gg \alpha, \quad 1 \le j \le M, \quad (2a)$$

and

$$X_i(t) > \beta|\nu_{j_i}|, \quad 1 \le i \le N, \quad (2b)$$

where ν_{j_i} are the components of the vector $\boldsymbol{\nu}_j$ [Eq. (A3)]. The coefficients $\alpha > 1$ and β serve to specify how many reactions occur and how many molecules exist within dt, respectively. Both α and β can vary with a system's size. For the simulations reported in Sec. IV, the values of α and β are based on trial and error. We tried the following combinations: $(\alpha, \beta) = \{(3000, 16\,000), (3000, 15\,000), (2000, 16\,000), (4000, 16\,000)\}$. Values of β less than $16\,000$ result in negative number of molecules of at least one component. Thus, values of β have a significant effect on classification of reactions as slow or fast. However, values of α have weaker effect as revealed by little change in computation time. This is because the range of α is wide so that these values are not critical in deciding fast or slow reactions. As a result, we found that $\alpha = 3000$ and $\beta = 16\,000$ provide good computational efficiency and maintain the positivity of the number of molecules.

Suppose that at a time t the system state is denoted as $\mathbf{X}(t)$, and the system consists of M_s slow and M_f fast reactions ($M_s + M_f = M$): $\mathcal{M} = \mathcal{M}_s \cup \mathcal{M}_f$, $\bar{\bar{\mathcal{M}}}_s = M_s$, and $\bar{\bar{\mathcal{M}}}_f = M_f$. Let the probability of the system state be denoted by $P[\mathbf{X}; t]$. Then, $P[\mathbf{X}; t]$ can be rewritten as the joint probability $P_{s,f}[\mathbf{X}; t]$, which is in turn expressed in terms of the conditional probability as $P_{s,f}[\mathbf{X}; t] = P_{s|f}[\mathbf{X}; t] P_f[\mathbf{X}; t]$. This allows one to approximate the rate of change of $P[\mathbf{X}; t]$,[47]

$$\frac{dP[\mathbf{X}; t]}{dt} = \frac{dP_{s|f}[\mathbf{X}, t]}{dt} P_f[\mathbf{X}; t] + \frac{dP_f[\mathbf{X}; t]}{dt} P_{s|f}[\mathbf{X}; t], \quad (3)$$

with

$$\frac{dP[\mathbf{X}; t]}{dt} \approx \frac{dP_f[\mathbf{X}; t]}{dt} P_{s|f}[\mathbf{X}; t]. \quad (4)$$

This approximation is justified by the fact that, at the time-scale of interest, slow reactions do not occur, and hence, $P_{s|f}[\mathbf{X}, t]$ does not change with time. So, its derivative is approximately zero.

The approximation in Eq. (4) provides a theoretical foundation[47] for the following hybrid strategy.

TABLE II. Criteria used to identify slow and fast reactions and corresponding numerical method. Columns 2 and 3 list the scale and simulation method in the scale (method) format.

# of molecules of species involved	Reaction propensity	
	High	Low
Large	Fast (CLE)	Slow (Gillespie)
Small	Slow (Gillespie)	Slow (Gillespie)

- Use the CLE to model fast reactions for which $a_j \tau$ ($j \in \mathcal{M}_f$) are large and the number of molecules of all the reactants is large to warrant the continuum approximation (see Appendix, Sec. 3).

- Employ the Gillespie algorithm to describe the remaining slow reactions. For the slow reactions, instead of Gillespie algorithm one can use the Gibson and Bruck's next reaction method[49] as the latter is about five times faster for the same level of accuracy.

These criteria for classifying reactions as slow or fast, and the corresponding numerical methods to be used to model each reaction, are summarized in Table II.

2. Deterministic modeling of nonreaction fluxes

Previously, Vasudeva and Bhalla[50] have used an adaptive approach to select between deterministic and stochastic approaches depending on the number of molecules involved.[51] However, in the present work, the need to use deterministic equations arises when one or more of the fluxes involved in the corresponding ODEs cannot be modeled as reactions. This does not depend on the number of molecules. Examples of such fluxes include complex interorganelle transport of molecules such as, in our model, movement of Ca^{2+} from endoplasmic reticulum to the cytosol through IP_3R channels [J_{ch} in Eq. (5)]. One can argue that this particular flux could be modeled using the 12 reversible reactions proposed by DeYoung and Keizer[52] and later simplified by Li and Rinzel.[45] However, in some cases the detailed mechanisms are not known and flux approximation is the only option.

The calcium dynamics model[3] includes four coupled ODEs for the state variables $[Ca^{2+}]_{ER}$, $[Ca^{2+}]_i$, h, and $[Ca^{2+}]_{mit}$, which contain fluxes whose underlying mechanisms involve many reactions that are not modeled explicitly. These processes are treated deterministically in our algorithms. Consider, for example, the rate of change of $[Ca^{2+}]_{ER}$ (the other three ODEs can be found here[3] and are provided in the supporting material[53]),

$$\frac{d[Ca^{2+}]_{ER}}{dt} = \frac{\beta_{ER}}{\rho_{ER}}(J_{SERCA} - J_{ch} - J_{ER,leak}). \quad (5)$$

In Eq. (5), the rapid binding of calcium to buffer proteins is modeled implicitly through β_{ER}, the ratio of free calcium to total (free and bound) calcium in the ER; and the use of ρ_{ER}, the volumetric ratio of the ER and the cytosol, obviates the need to specify the ER volume explicitly. The calcium fluxes through the SERCA pump back to the ER, J_{SERCA}, through the IP_3R channel from the ER to the cytosol, J_{ch}, and due to

the calcium leakage from the ER, $J_{ER,leak}$, are prescribed as nonlinear functions of the state variables $[Ca^{2+}]_{ER}$, $[Ca^{2+}]_i$, h, and $[Ca^{2+}]_{mit}$.

The complexity of the fluxes of the state variables $[Ca^{2+}]_{ER}$, $[Ca^{2+}]_i$, h, and $[Ca^{2+}]_{mit}$ complicates their modeling with the stochastic simulation algorithms described above. For example, the expression for J_{ch} is given by

$$J_{ch} = v_{max,ch} \times \left(\left[\frac{[IP_3]}{[IP_3] + K_{IP3}} \right] \times \left[\frac{[Ca^{2+}]_i}{[Ca^{2+}]_i + K_{act}} \right] \times h \right)^3$$
$$\times ([Ca^{2+}]_{ER} - [Ca^{2+}]_i). \quad (6)$$

So, in our hybrid approach, the corresponding four ODEs are integrated via a first-order Euler scheme after all other quantities are updated using the multiscale stochastic method described in Sec. III C 1. The coupling of continuum (ODE-based) and stochastic (particle-based) descriptions requires relating the concentrations to numbers of molecules. For the cytosolic calcium dynamics in RAW 264.7 cells considered in this study, we use a cytosolic volume $V = 10$ pL or a cell diameter of 27 μm. Then the concentrations, e.g., the concentration of ligand, $[L] = 30$ nM, can be related to the numbers of molecules, as follows:

$$30 \text{ nM} = 30 \times 10^{-9} \times \frac{6.022 \times 10^{23}}{L}$$
$$\times 10^{-11} \text{ L} = 180\,660 \text{ molecules}. \quad (7)$$

3. Reactions with complex rate expressions

Some explicitly modeled reactions have complex rate laws which are actually functions of Michaelis–Menten (MM) or Hill dynamics-based complex rate expressions.

We studied four methods for stochastic simulation presented in the literature to perform coarse-graining and handling complex rate laws for a single reaction and coupled reactions with Michaelis–Menten kinetics. The first such contribution is the quasi-steady-state approximation (QSSA) approach of Rao and Arkin.[8] Mastny *et al.*[54] have carried out in-depth analysis of using QSSA under different conditions through the use of singular perturbation analysis. More recently, Barik *et al.*[13] have extended the QSSA by analyzing the conditions under which the standard QSSA might fail. They have utilized the total QSSA (TQSSA) and have shown that under certain conditions the method of Rao and Arkin[8] fails. They have applied the TQSSA approach to a single Michaelis–Menten mechanism, the Goldbeter–Koshland (GK) ultrasensitive switch system involving two coupled Michaelis–Menten mechanisms, and a bistable system composed of two GK switches. The approach requires solving quadratic equations to solve for the propensity of slow reactions for use with the standard Gillespie algorithm. For these cases, the results are outstanding in that the mean temporal responses obtained from the TQSSA and the standard Gillespie algorithm are indistinguishable. The work of Gillespie *et al.*[18] deals with a detailed analysis of the issues in simplification of Michaelis–Menten formulation into a single-step reaction in stochastic simulation.

All these are successful approaches in handling systems with one or a few reactions. However, these approaches have not been applied to more complex systems involving many reactions (say, about 20 or more) with both simple and complex rate laws. In our case, some of the rate laws are significantly more complex than the examples presented in these contributions. Also, in our case, the corresponding mechanisms are highly lumped representations of the underlying detailed mechanisms. If one were to consider the detailed mechanisms, the parameters would be unknown, making the simulations infeasible.

To handle such rate laws, here we provide an example of the calculation of the propensity functions [Eq. (A2)] for such reactions; other reactions are treated similarly in the supporting material (Table S2).[53]

We consider the forward component of the lumped-enzymatic reaction 3 in box 1 of Fig. 1(b) (reaction 5 in Table S1 of supporting material),[53]

$$[GRK;Ca_i]LR \xrightarrow{k_{f,3}} LRp, \qquad (8)$$

which is facilitated by the presence of enzymes GRK and Ca_i. The corresponding flux can be written as[3] (see also Tables S1 and S2 in supporting material)[53]

$$v_5 = k_{f,3}[LR][GRK]MM_f(K_{m,Ca_i,3},[Ca^{2+}]_i), \qquad (9)$$

where $k_{f,3}$ is second-order rate constant, $K_{m,Ca_i,3}$ is the Michaelis parameter, and $MM_f(K_m,x)=x/(K_m+x)$ is the MM rate expression. Recognizing that LR acts as a reactant and recalling Eq. (A2), we compute the propensity function a_5 for reaction of Eq. (8) by first determining the number of possible combinations of reactant molecules in the reaction of Eq. (8) as $h_5=[LR]N_AV$ and the corresponding specific probability rate constant as $c_5 =k_{f,3}[GRK]MM_f(K_{m,Ca_i,3},[Ca^{2+}]_i)$. Hence, the propensity function $a_5=c_5h_5$ is given by

$$a_5 = v_5N_AV. \qquad (10)$$

Another example is given in Sec. 1.3 of supporting material. Analysis similar to that leading to Eq. (10) and Eq. (S12) of supporting material suggests the following relationship between the propensity function and the macroscopic flux of a jth reaction with a complex rate expression:

$$a_j = v_jN_AV. \qquad (11)$$

The stepwise procedure for numerical implementation of the entire multiscale hybrid stochastic simulation is presented in the supporting material.[53]

D. Application to cytosolic calcium dynamics in RAW cells

This multiscale hybrid approach was applied to the cytosolic calcium dynamics with parameter values and initial conditions taken from Maurya and Subramaniam.[3] The system consists of 28 irreversible reactions and 26 species [Table S1 and Eq. (1) in Supporting Material[53]], which are represented by the state vector,

$$\mathbf{X} = [L,R,LR,G_{\beta\gamma},GRK,GRK . G_{\beta\gamma},Ca_i^{2+},LR_p,R_p,LR_i,ARR,$$
$$R_{p,i},R_{pool},G_iD,T,G_{\alpha,i}T,G_{\alpha,i}D,A,PIP_2,IP_3,PLC_\beta,IP_{3,p}$$
$$X_{PIP2,gen},CaM,Ca2.CaM,Ca2.CaM . GRK]^T. \qquad (12)$$

The multiscale hybrid algorithm is needed because the numbers of molecules of some of these species are close to 0 while others have above 10^6 molecules (Table S3 in supporting material[53]) and because the propensity functions $a_j(\mathbf{X})$ ($j=1,\ldots,28$) vary from 0 to over 10^4.

Before the ligand is added, the system is simulated for 1000 s so that the system reaches a steady state. At time $t =1000$ s, ligand C5a is applied to cells and binds to its receptor (C5aR), which leads to the increase in IP_3 levels. The simulation consists of two phases: before adding ligand and after adding ligand. At $t=0$, the species R, $G_{\beta\gamma}$, GRK, Ca_i^{2+}, R_{pool}, T, $G_{\alpha,i}D$, A, PIP_2, PLC_β, $X_{PIP2,gen}$, and CaM are present (Table S3 in supporting material[53]). Other species have zero molecules.

At the first time step, $\tau=8.0361\times10^{-7}$ s. Reactions 14, 17, 18, and 21 in Fig. 1(b) are considered to be fast, while the remaining reactions are taken to be slow (see approximation 2b). The second time step is calculated based on the reaction rates, number of molecules obtained from first time step, etc.

All simulations reported in Sec. IV were carried out on the linux-based Triton Cluster at San Diego Supercomputer Center (SDSC), with parallelization accomplished by using Microsoft's STAR-P program. The number of processors used varied between 8 and 256 depending on the number of realizations generated. On an average, the simulation time for each realization was 15 h. The total single-processor equivalent of simulation time for all the results is about 50 000 h.

IV. RESULTS

Comparison of response of $[Ca^{2+}]_i$ from stochastic and deterministic simulation is presented in Sec. II A and Fig. S1 of Supporting material. Comparison of results from stochastic simulation and single-cell calcium measurements by the Alliance for Cellular Signaling are presented in Sec. II B and Fig. S2 of Supporting material. As evident from Fig. S1F, in the limit of large number of molecules of reacting species, stochastic and deterministic simulations yield nearly identical results. Below, we compare other features of the response as predicted by stochastic versus deterministic simulation.

A. Dose response

Dose response, which is a measure of efficacy of a ligand,[3] is presented in Fig. 3. Rather than relying on commonly used saturating dose levels to generate dose-response curves, we choose only sub-basal (very low) doses. This enables us to identify differences between the dose responses of $[Ca^{2+}]_i$ predicted by deterministic and stochastic simulations, respectively. Figure 3(a) demonstrates the temporal evolution of the dose responses of $[Ca^{2+}]_i$ to the basal dose of $[C5a]=30$ nM and its 0.1%, 1%, 10%, and 50% fractions. The peak-height of cytosolic Ca^{2+} increases with the dose of ligand, a finding that is made explicit in Fig. 3(c).
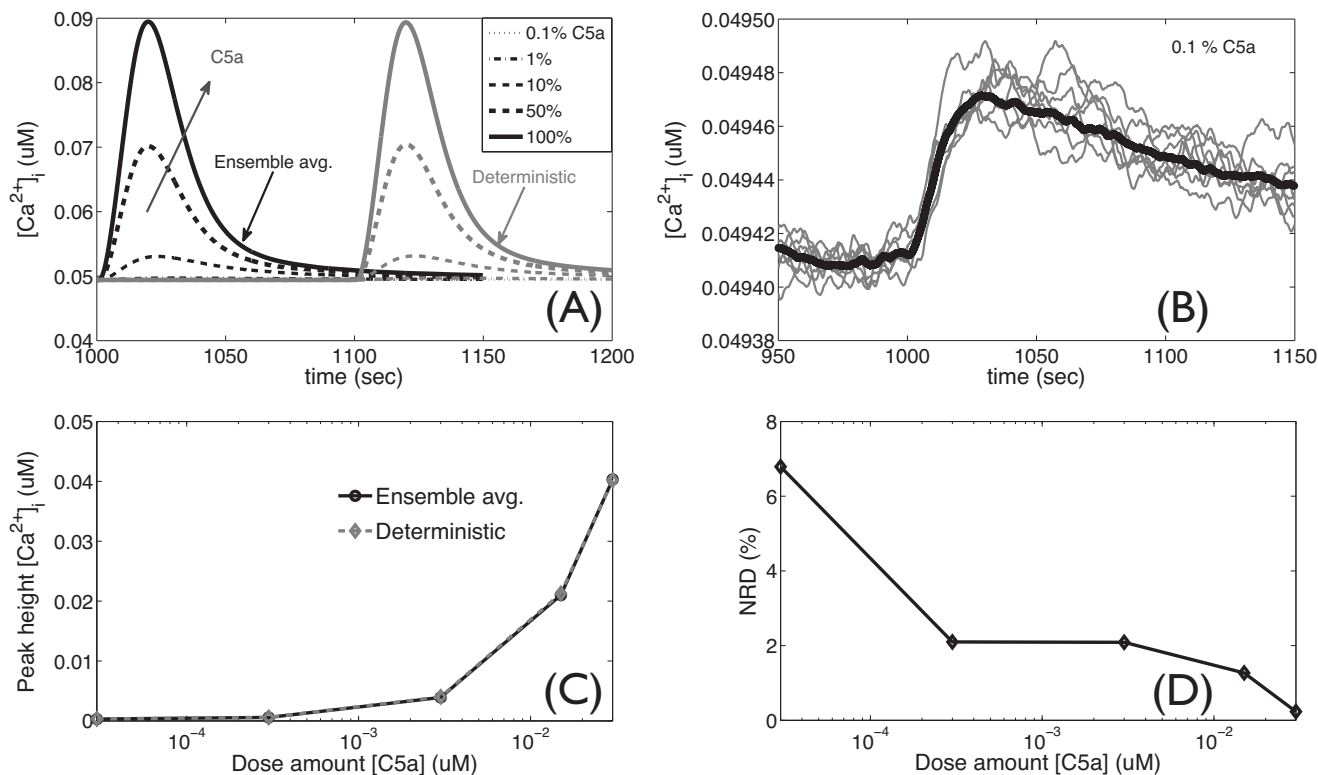
FIG. 3. Dose response. (a) Comparison between ensemble average of 16 realizations and deterministic simulation. For better contrast, the time-course from deterministic simulation is shifted by 100 s. (b) Comparison between ensemble average and individual realizations in stochastic simulation for 0.1% (of 30 nM) strength of the ligand C5a. (c) Comparison of the dose response (peak-heights): The difference is quite small as compared to the scale of peak-height. (d) At lower doses, the NRD is larger indicating the stochastic effects. The NRD decreases with increasing dose as the number of the molecules of C5a becomes several hundreds or more.

The stochasticity effects and differences in $[Ca^{2+}]_i$ responses obtained from the deterministic and stochastic simulations are explored in Figs. 3(b) and 3(c). Note that in Fig. 3(a) the dose responses computed with the two approaches are nearly identical, with the deterministic predictions shifted to the right by 100 s to improve visibility. Figure 3(b) demonstrates the importance of stochasticity (randomness) for small numbers of ligand molecules (e.g., 0.1% C5a), when the peak-height varies substantially between realizations. Although the ensemble mean of the peak-height of $[Ca^{2+}]_i$ response from these realizations visually overlaps with that from deterministic prediction, quantitatively, they are different as expressed through "normalized response difference (NRD)" in Fig. 3(c).

As the number of molecules becomes very small, the concept of "concentration" loses its rigor and deterministic simulations can be expected to introduce modeling errors. This effect is elucidated in Fig. 3(d), where the relative error or (NRD) ($\mathcal{E}$) between the deterministic and stochastic solutions of $[Ca^{2+}]_i$ response is shown. $\mathcal{E}$ is computed as

$$\mathcal{E} \equiv \frac{|\text{deterministic} - \text{ensemble avg}|}{\max(\text{deterministic}, \text{ensemble avg})} \times 100\%. \quad (13)$$

Figure 3(d) shows that $\mathcal{E}$ decreases as the dose of C5a increases, indicating the diminishing effects of randomness (stochasticity). The NRD varies from $\mathcal{E}=7\%$ at the 0.1% dose to almost zero at the full dose of 30 nM. These results demonstrate that at lower doses, stochastic simulations are needed and that the ensemble average of multiple realiza-

tions provides a more accurate prediction of the system behavior then does the deterministic output. Further analysis of this phenomenon is presented below.

B. Convergence of stochastic simulations at low doses

Figures 4(a)–4(d) show the histograms of the peak-value of calcium response, $[Ca^{2+}]_i$, due to the 0.1% dose of C5a. The histograms in Figs. 4(a)–4(d) represent, respectively, 16, 64, 256, and 512 realizations of the stochastic hybrid algorithm, using 20 bins in each case. The vertical dotted line in each panel corresponds to the mean computed from the corresponding number of realizations, and the solid curves are the Gaussian distributions whose mean and variance are computed from the same realizations. Although the central limit theorem applies to the distribution of the mean of a random variable instead of the distribution of the random variable itself, it is interesting to note that the shape of the computed distributions approaches the Gaussian distribution as the number of realizations increases from 16 in Figs. 4(a) to 512 in Figs. 4(d).

To find out if the central limit theorem is applicable to the peak-value of $[Ca^{2+}]_i$ response, the mean of 4, 8, 16, or 32 realizations was computed. This was repeated in each case to generate 1024 such mean values. The histogram of the mean values is shown in Figs. 4(e)–4(h). All the four histograms are similar to a Gaussian distribution and the
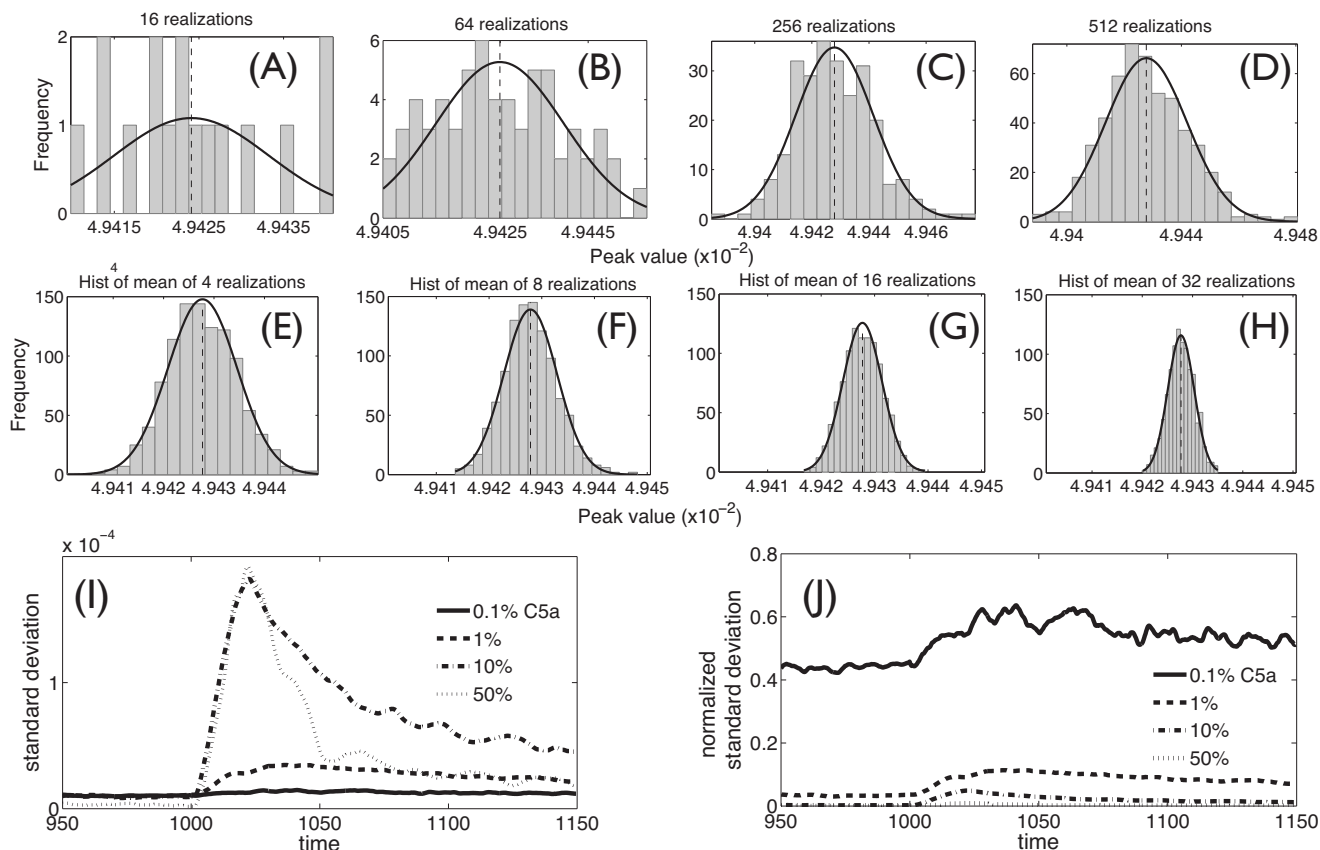
FIG. 4. Revelation of stochastic effects at low doses. (a)–(d) Distributions of peak-height for the 0.1% dose of C5a computed from 16, 64, 256, and 512 realizations, respectively. The dotted vertical line represents the mean value and the solid curves denote theoretical Gaussian distributions. As the number of realizations increases, the shape of the histogram approaches a Gaussian distribution. (e)–(h) The mean of 4, 8, 16, or 32 realizations was computed and 1024 such mean values were generated. All the four histograms are similar to a Gaussian distribution and the standard deviation from these distributions indeed decreased proportional to $1/\sqrt{N_r}$, N_r being the number of realizations used to compute the mean. (i) The standard deviation computed from 16 realizations for several doses. Contrary to the expectation, higher doses result in larger absolute standard deviations. (j) The normalized standard deviation decreases as the dose is increased, signifying the effect of randomness at lower doses.

standard deviation from these distributions indeed decreased proportional to $1/\sqrt{N_r}$, N_r being the number of realizations used to compute the mean.

C. Random variability of the $[Ca^{2+}]_i$ response at low doses

The number of molecules of C5a at 0.1% dose is about 180. The number of molecules of cytosolic Ca^{2+} is of the order of 300 000. The number of molecules of free $G_{\beta\gamma}$ is about 10 000 and that of the phosphorylated receptor still bound to the ligand (LR_p) is about 60. Figure 4(i) shows how standard deviation (σ) of the $[Ca^{2+}]_i$ response varies across 16 realizations. Figure 4(j) shows the variation of the normalized standard deviation $\tilde{\sigma}$, defined as: $\tilde{\sigma} = \sigma/H$, where $H = h - b$ is the difference between the basal level of calcium response b and the peak level h. It is clear from Fig. 4(j) that the normalized standard deviation $\tilde{\sigma}$ increases as the C5a dose decreases, indicating the increasing importance of randomness (stochasticity). This is because as the C5a dose (the number of C5a molecules) decreases, fewer C5a molecules participate in chemical collisions and hence the enhanced relative importance of stochasticity. One implication of this is that more stochastic realizations are needed to accurately estimate the mean response or the variability in response.

From an experimental view point, a larger population of cells is needed to get a stable readout for mean calcium response.

D. Sensitivity analysis

In this study we have focused on the perturbations in the initial pool of certain species. Quantification of parametric uncertainty in the reaction rate constants used in the Gillespie and other algorithms described above can be carried out following the procedure described by Srinivasan *et al.*[55] A similar analysis could be performed with respect to perturbations in the rate parameters while keeping the C5a dose and the initial pool of all species at their nominal levels. Since the number of molecules is sufficiently large under these conditions, the results of sensitivity analysis using stochastic simulation are similar to those obtained using deterministic simulation. As an example, results of sensitivity analysis of $[Ca^{2+}]_i$ response for changes in k_1 are shown in Fig. S3 in the supporting material.[53]

The sensitivity of $[Ca^{2+}]_i$ response to variations in IC:$[G_{\beta\gamma}]$ is shown in Fig. 5 and for IC:$[R]$ and IC:$[G_{\alpha,i}D]$ is shown in Fig. S4 (supporting material). In this discussion, IC refers to initial condition, which is generally also the total pool of protein/species being considered. These concentrations were changed, one at a time, by factors of 10^{-3}, 10^{-2},
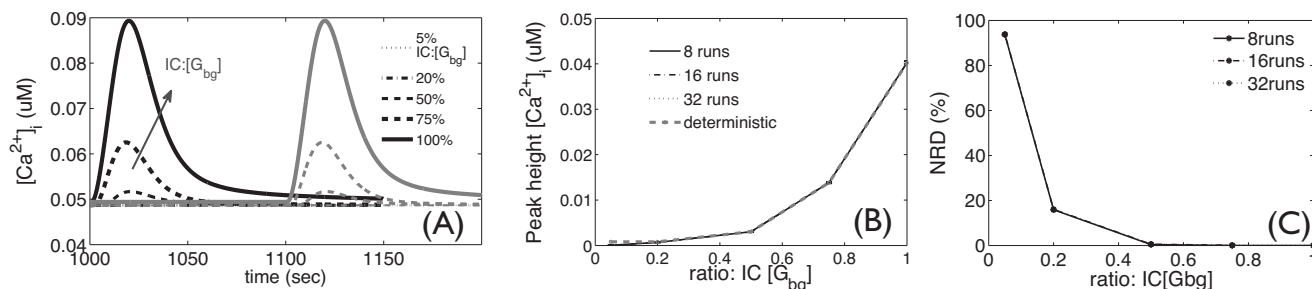
FIG. 5. Sensitivity analysis. (a)–(c) *Response of* $[Ca^{2+}]_i$ *to changes in* IC:$[G_{\beta\gamma}]$. The decrease in the peak-height due to decrease in IC:$[G_{\beta\gamma}]$ is much more pronounced than that caused by the same decrease of IC:$[R]$. (c) NRD $\mathcal{E}$ is extremely high at very low IC:$[G_{\beta\gamma}]$, suggesting significant stochastic effects at low numbers of molecules of $[G_{\beta\gamma}]$. (b) and (c) also show the effect of using different numbers of realizations for computing the mean. Such differences are small (see text) indicating that 16 realizations are sufficient for computing the mean.

0.05, 0.1, 0,2, 0.5, and 0.75 of their respective base values. For each concentration change, a new basal level (steady state) was computed by allowing the system to evolve for 1000 s before ligand addition, at which time 30 nM of C5a ligand was applied. Note that 10% of a base value means a 90% knockdown of the species/gene in question. Shift of basal level before ligand addition and the peak-height from basal level are the main focus of this sensitivity analysis.

Figures 5(a)–5(c) provide an analysis of the $[Ca^{2+}]_i$ response to changing doses of IC:$[G_{\beta\gamma}]$, which varies from its base value to the 1/20, 1/5, 1/2, and 3/4 fractions thereof. The number of molecules involved at 1/20 level of IC:$[G_{\beta\gamma}]$ is: $G_{\alpha,i}D$: 46 000, $G_{\alpha,i}T$: 5100, free $G_{\beta\gamma}$: 16, GRK.$G_{\beta\gamma}$: 10, LR_p, 1400, R_p, 15, IP$_3$: 260 000, and free cytosolic Ca^{2+}: 290 000. Figures 5(b) and 5(c) reveal that the $[Ca^{2+}]_i$ response is very sensitive to the changes in IC:$[G_{\beta\gamma}]$. Its peak-height decreases by 90% as IC:$[G_{\beta\gamma}]$ is reduced by 50% and becomes negligible when $[G_{\beta\gamma}]$ drops below 20% of its base value [Fig. 5(b)]. The relative error between the $[Ca^{2+}]_i$ responses predicted by deterministic and stochastic simulations, $\mathcal{E}$ [Fig. 5(c)], becomes very large when the concentration $[G_{\beta\gamma}]$ drops below 20% of its base value, indicating the importance of randomness, which is caused by small numbers of molecules of $G_{\beta\gamma}$.

We have also studied how the mean peak-height and NRD change when different numbers of realizations are used. Figure 5(b) shows the mean peak-height obtained from 8, 16, 32 realizations and deterministic simulation. The curves are almost indistinguishable. Difference for [5%, 20%, 50%, 75%, 100%] of IC:$[G_{\beta\gamma}]$ is [1.18 0.16 0.16 0.10 0.10]%; the largest difference being less than 1.2%. Essentially, 16 realizations are sufficient to compute the mean with good accuracy. So, 16 realizations are used in other simulations as well.

E. Calcium response to protein knockdown

Since the stochastic hybrid algorithm enables us to predict cytosolic calcium dynamics when only a few molecules of reacting species are present, we are in a position to explore the effects of proteins' knockdown on calcium response. Figures 6 and 7 show the $[Ca^{2+}]_i$ response to knockdown of proteins PLCβ and GRK, respectively. Figure 8 shows the $[Ca^{2+}]_i$ response to knockdown of protein GRK and perturbation of (knockdown of the protein related to)

$V_{max,PM,IP3dep}$. To model a protein's knockdown, we first reduced its basal level, and then computed a new basal level (steady state) by evolving the system for 1000 s, at which time 30 nM of C5a ligand was applied.

Figures 6(a) and 6(b) show the $[Ca^{2+}]_i$ response to the 50%, 80%, 90%, and 99% knockdown of PLCβ for 0.1% and 10% doses of IC:$[R]$, respectively. The number of molecules involved at 0.1% dose of IC:$[R]$ and 90% knockdown of PLCβ is total PLCβ: 3400, $G_{\alpha,i}D$: 17 000, $G_{\alpha,i}T$: 350, free $G_{\beta\gamma}$: 14 000, GRK.$G_{\beta\gamma}$: 3700, LR_p, 225, R_p, 2, IP$_3$: 270 000, and free cytosolic Ca^{2+}: 297 000. Figure 6(c) shows the variation of the $[Ca^{2+}]_i$ peak-heights corresponding to different combinations of the PLCβ and IC:$[R]$ levels. Both the peak-height and basal levels of $[Ca^{2+}]_i$ decrease as the knockdown level of PLCβ increases. The deterministic and stochastic simulations yield similar results with NRD less than 4% [Fig. 6(d)]. This clearly suggests that it may not be necessary to carry out stochastic simulation to model knockdown of PLCβ. For experiments, the implication is that a relatively smaller population of cells may be sufficient to get a stable readout if other experimental factors can be controlled.

Figures 7(a) and 7(b) present the $[Ca^{2+}]_i$ response to the 50%, 80%, 90%, and 99% knockdown of GRK for 0.1% and 10% doses of IC:$[R]$, respectively. The number of molecules involved at 0.1% dose of IC:$[R]$ and 90% knockdown of GRK is free GRK: 1500, $G_{\alpha,i}D$: 9200, $G_{\alpha,i}T$: 400, free $G_{\beta\gamma}$: 10 000, GRK.$G_{\beta\gamma}$: 400, LR_p, 44, R_p, 1, IP$_3$: 400 000, and free cytosolic Ca^{2+}: 301 000. The largest peak-height occurs at lowest $[GRK]$ and highest $[R]$ [Fig. 7(c)], which is qualitatively opposite to the response due to the PLCβ. Figure 7(d) demonstrates that either deterministic or stochastic simulations can be used to investigate this behavior, with the maximum NRD $\mathcal{E}$ of about 1.5%, which occurs at low $[R]$ and is practically independent of the level of GRK.

Figure 8 demonstrates the $[Ca^{2+}]_i$ response to various degrees of simultaneous knockdown of protein GRK and the protein related to $V_{max,PM,IP3dep}$. Knockdown of GRK has a more pronounced effect on $[Ca^{2+}]_i$ response than does $V_{max,PM,IP3dep}$. The relative importance of the two knockdowns does not change at different levels of KD. This suggests the robustness of the system response over a large range of perturbations.
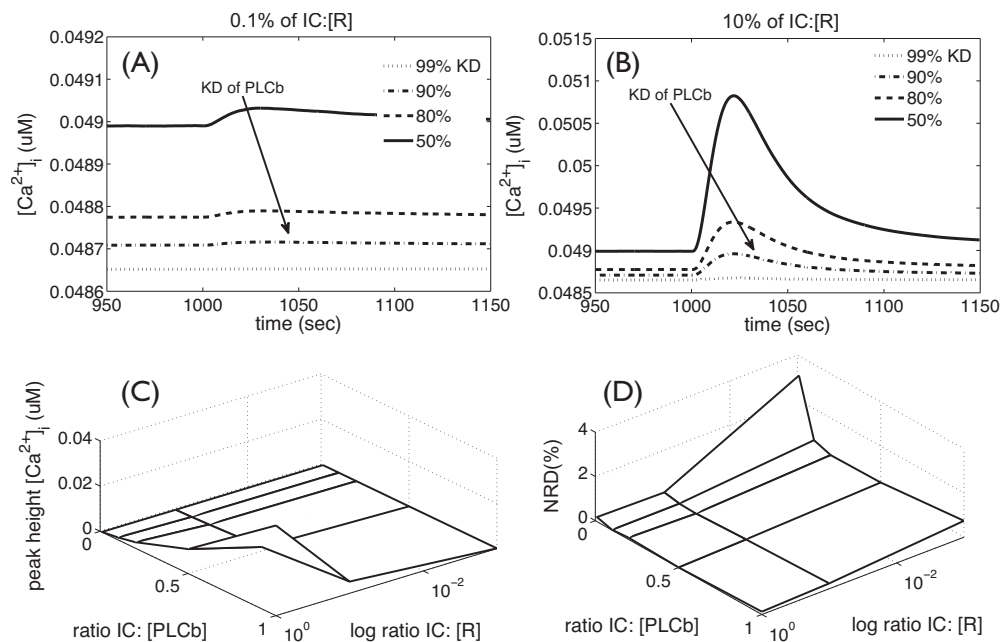
FIG. 6. Knockdown response of PLCβ. [(a)–(b)] The $[Ca^{2+}]_i$ response to the 50%, 80%, 90%, and 99% knockdown of PLCβ for 0.1% and 10% levels of IC:[R], respectively. As the knockdown rate of PLCβ increases, both the basal level and peak-height of $[Ca^{2+}]_i$ decrease because the IP$_3$ production decreases due to decrease in PLCβ. (c) Peak-height of $[Ca^{2+}]_i$ response corresponding to different combinations of the PLCβ and IC:[R] levels. Peak-height increases with high amount of IC:[R] and [PLCβ]. (d) NRD $\mathcal{E}$ is insignificant and decreases as doses of R and PLCβ increase.

V. SUMMARY AND DISCUSSION

In summary, we have integrated the existing techniques for multiscale stochastic simulation with deterministic simulation to deal with complex reaction systems and have applied it to studying calcium dynamics in macrophage cells. When the concentration of reactants is sufficiently large, the stochastic method yields time-course profiles identical to those obtained from a deterministic model (ensemble aver-

age of 16 or more realizations). However, at lower number of molecules of one or more species, measurable relative difference in $[Ca^{2+}]_i$ responses predicted by the two approaches is obtained, especially for the case of G$_{\beta\gamma}$, thus suggesting the necessity of using stochastic simulation as opposed to deterministic simulation for studying system dynamics at subcellular levels. Dose response analysis revealed that while the NRD between $[Ca^{2+}]_i$ responses predicted by deterministic
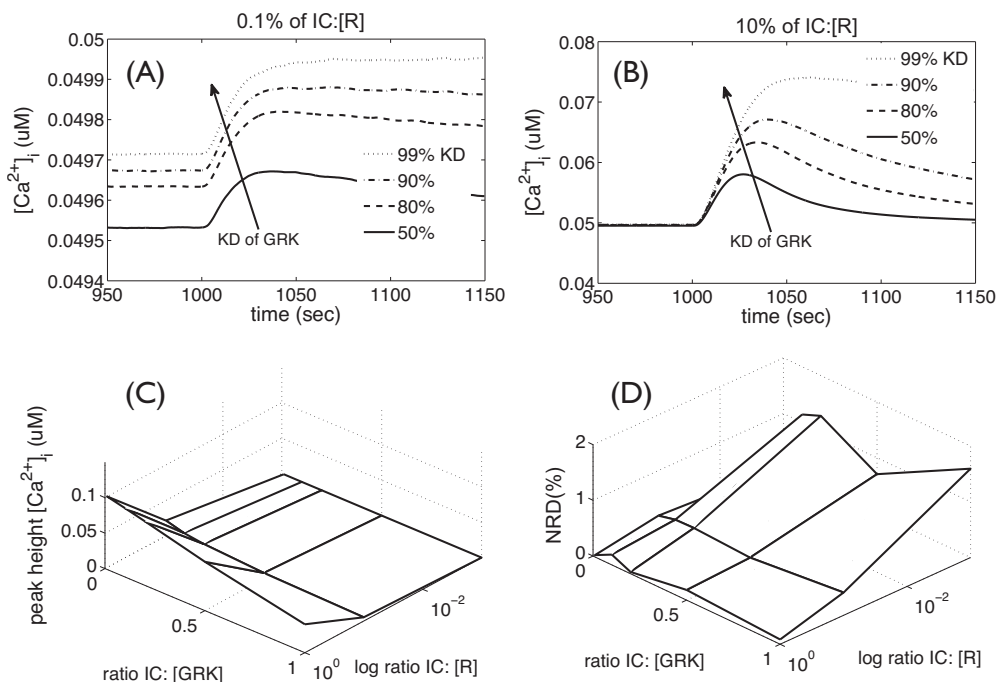

FIG. 7. Knockdown response of GRK. [(a) and (b)] The $[Ca^{2+}]_i$ response to the 50%, 80%, 90%, and 99% knockdown of GRK for 0.1% and 10% levels of IC:[R], respectively. (c) Peak-height of $[Ca^{2+}]_i$ response corresponding to different combinations of [GRK] and IC:[R] levels. (d) NRD $\mathcal{E}$ is insignificant, reaching its maximum of about 1.5% at low IC:[R].
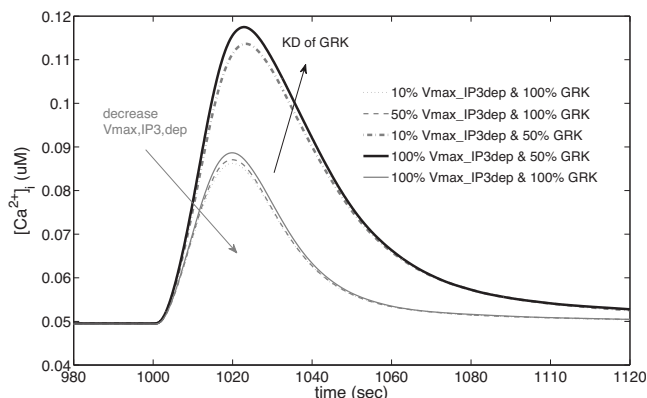
FIG. 8. The $[Ca^{2+}]_i$ response to the simultaneous knockdown of GRK and gene/protein related to $V_{max,IP3dep}$. Knockdown of GRK and reduction of $V_{max,PM,IP3dep}$ have opposite effects on the $[Ca^{2+}]_i$ response. The response is much more sensitive to knockdown of GRK than to decrease in $V_{max,PM,IP3dep}$.

and stochastic simulations is negligible at the full dose of 30 nM (shown) or higher doses including saturating doses (not shown), it increases with decreasing doses. At 0.1% dose, it is as high as 7%. These results are emphasized again in the sensitivity analysis of the parameters used in the simulation and in the knockdown analysis of reacting protein components.

A. Methodological components

We have developed a hybrid approach to stochastic simulation, in which slow reactions and fluxes are handled through exact stochastic simulation and their fast counterparts are treated partially deterministically through the chemical Langevin equation. The classification of reactions as fast or slow is accompanied by the assumption that in the time-scale of fast reactions, slow reactions do not occur and hence do not affect the probability of the state. Our new approach also handles reactions with complex rate expressions such as functions of Michaelis–Menten kinetics and power-law kinetics by developing mathematical expressions for their propensity functions and microscopic fluxes. Fluxes which cannot be modeled explicitly through reactions are handled deterministically.

B. Sensitivity analysis

The peak-height of the $[Ca^{2+}]_i$ response decreases with decreasing value of $IC:[G_{\beta\gamma}]$, and no baseline shift is observed [Fig. 5(a)]. In the absence of perturbation, at early times, the concentrations $[G_{\beta\gamma}]=8.28e^{-3}$ μM and $[G_{\alpha,i}D]=8.12e^{-3}$ μM are almost equal. However, if $IC:[G_{\beta\gamma}]$ is decreased, there is little free $G_{\beta\gamma}$ left. Since this directly affects the rate of PIP_2 hydrolysis, no IP_3 can be generated. Due to this effect, with decreasing $IC:[G_{\beta\gamma}]$, the peak-height of $[Ca^{2+}]_i$ decreases much more sharply. Although not shown in Figs. 5(a) and 5(b), if $IC:[G_{\beta\gamma}]$ increases beyond 100% of base case, then the excess $G_{\beta\gamma}$ is present in the free form, hence both the basal level and peak-height increase until saturation. This is similar to the decrease in $IC:[G_{\alpha,i}D]$ shown in Figs. S4 D-F (supporting material) and briefly discussed below.

With decreasing $IC:[R]$, lesser $[G_{\beta\gamma}]$ is available[28] (Figs. S4 A-C, supporting material), which results in reduced activation of $PLC\beta$ and as a consequence reduced hydrolysis of PIP_2 into IP_3. Hence, the increase in cytosolic $[Ca^{2+}]$ is smaller. The sensitivity curve for $IC:[R]$ in Fig. S4 B is non-linear. This is because the ligand and the receptor bind in 1:1 stoichiometry and the nominal value of $IC:[R]$ (~40 nM) are larger than the nominal (100%) level of C5a (30 nM). Thus, for a small decrease (say, 10%) in $IC:[R]$, about 36 nM $[R]$ is present. Since 36 nM is still larger than 30 nM, the dynamics of $[LR]$ remains almost the same and so does the peak-height of the temporal response of $[Ca^{2+}]_i$. Basal level does not change in our model since the receptor comes into play only after adding the ligand. In reality, there is a little decrease of $[Ca^{2+}]$ in cytosol due to the little basal activity, but it is compensated by the basal hydrolysis rate of PIP_2 and hence is unobservable.

Sensitivity analysis of $IC:[G_{\alpha,i}D]$ shows biphasic response of $[Ca^{2+}]_i$: large baseline shift and low peak-height at substantially low $IC:[G_{\alpha,i}D]$ (supporting material, Fig. S4 D, upper panel) and a small baseline shift (increase) and the corresponding nominal increase of peak-height at relatively smaller perturbations ([90% 85% 80%] of $IC:[G_{\alpha,i}D]$, Fig. S4 D, lower panel). At substantially low $[G_{\alpha,i}D]$, large amount of free $[G_{\beta\gamma}]$ results in a large basal level shift, and with the basal level at this plateau, little additional increase in $[Ca^{2+}]_i$ is observed, i.e., this results in a low peak-height of $[Ca^{2+}]_i$ upon ligand addition.

The NRD increases with decreasing $IC:[R]$. The behavior of NRD for decrease in $IC:[G_{\beta\gamma}]$ is similar to that for decrease in $IC:[R]$ except that it is drastically larger at very low values (more than 80% NRD at 5% $IC:[G_{\beta\gamma}]$). While the NRD in the sensitivity analysis of $IC:[R]$ is under 2% for all changes, it is up to 90% in the perturbation of $IC:[G_{\beta\gamma}]$. There are three reasons for this drastic difference: (1) stochastic effects are prominent at low concentrations, (2) the system is very sensitive to large decreases in $[G_{\beta\gamma}]$ as compared to in $[R]$ or $[G_{\alpha,i}D]$, and (3) the NRD is normalized by the peak-height [Eq. (13)]. Since peak-height is very low at low $[G_{\beta\gamma}]$, the NRD gets amplified.

C. Knockdown (KD) analysis

Our results show reduced G-protein activity and $[Ca^{2+}]_i$ response upon KD of the receptor. KD of $G_{\beta\gamma}$ results in a sharp decrease in calcium levels and KD of $G_{\alpha,i}D$ results in considerably large increases in basal level of $[Ca^{2+}]_i$ (inferred from sensitivity analysis). KD of GRK results in increased and prolonged mobilization of calcium since the receptor remains active for a longer time. Thus, GRK regulates G-protein activity strongly. Similar to $G_{\beta\gamma}$, knockdown of $PLC\beta$ shows a sharp decrease in $[Ca^{2+}]_i$. This is because IP_3 generation is catalyzed by the active complex of Ca^{2+}, $PLC\beta$, and $G_{\beta\gamma}$. As the knockdown level of $PLC\beta$ increases, both the peak-height and basal levels of $[Ca^{2+}]_i$ decrease since less IP_3 is generated [reaction 18 in Fig. 1(b)]. Qualitatively, the knockdown response of $PLC\beta$ is similar to that of the knockdown response of $G_{\beta\gamma}$ since both play a similar role in IP_3 generation [modules 2 and 3 in Fig. 1(b)].

TABLE III. Summary of results of KD response. The change in the features of calcium response listed is for increase in KD-level (decrease in IC:[.] of the protein). Qualitative nature of the features is mostly independent of the level of [R].

Protein/variable name	Basal level	Peak-height
PLCβ	Decreases	Decreases, convex
GRK	Very small increase	Increases, linear
$V_{\text{max,PM,IP3dep}}$	No change	Small decrease

In contrast to the KD response of PLCβ, as KD level of GRK increases, peak-height of $[\text{Ca}^{2+}]_i$ increases strongly [Figs. 7(a) and 7(b)]. This is because the phosphorylation induced through reactions 3 and 4 decreases as KD level of GRK increases [Fig. 1(b)]. Moreover, the time to return to steady state also increases considerably since the receptor remains active for a longer time and relatively more $G_{\beta\gamma}$ is present in the free active state. The basal level increases slightly relative to peak-height only at low IC:[R] [0.1%, Fig. 7(a)]. At moderate IC:[R] [10%, Fig. 7(b)], the increase in basal level is negligible as compared to the peak-height.

$V_{\text{max,PM,IP3dep}}$ affects $J_{\text{PM,IP3dep}}$ (IP$_3$-dependent in-flux to cytosol across the plasma membrane) in a proportional manner. Double perturbation of GRK and $V_{\text{max,PM,IP3dep}}$ has revealed that for increase in their KD levels, GRK and $V_{\text{max,PM,IP3dep}}$ have opposite effects on $[\text{Ca}^{2+}]_i$. Reduction of $V_{\text{max,PM,IP3dep}}$ results in decrease of $[\text{Ca}^{2+}]_i$ because $J_{\text{PM,IP3dep}}$ is reduced (the lower three time-courses shown with light colored lines in Fig. 8). On the contrary, KD of GRK increases $[\text{Ca}^{2+}]_i$ response because phosphorylation of the active receptor is reduced [Fig. 8, time-course shown with light continuous line (100% $V_{\text{max,PM,IP3dep}}$ and 100% GRK) and time-course shown with dark continuous line (100% $V_{\text{max,PM,IP3dep}}$ and 50% GRK)]. The qualitative nature of the response does not change at different KD levels of the protein GRK and the protein related to $V_{\text{max,PM,IP3dep}}$ suggesting that the system is robust to such perturbations.

The main features of the KD response are summarized in Table III.

D. Stochastic effects at low molecular numbers

In the base case (30 nM C5a), there is good agreement between $[\text{Ca}^{2+}]_i$ responses predicted by deterministic and stochastic simulation. However, at low doses of the ligand or proteins such as the receptor and GRK, stochastic effects become prominent resulting in up to 2%–4% NRD for low concentrations of the receptor, GRK and $G_{\alpha,i}$D, up to 7% NRD for dose response and up to 90% NRD for low concentration of $G_{\beta\gamma}$. Although the absolute value of fluctuations is larger in the case of higher doses resulting in a higher peak $[\text{Ca}^{2+}]_i$ value, the normalized standard deviation of the response increases with decreasing dose.

E. Deriving statistics from stochastic simulation

We also found that with more realizations, the computed distribution of the ensemble mean of the peak-height approaches a normal distribution when the number of realizations used to compute the mean increases, as would be mandated by the central limit theorem. The standard error of mean decreases proportional to inverse of the square root of the number of realizations used to compute the mean. Statistics related to low order moments of the distribution, such as mean and standard deviation, could be computed accurately with relatively small number of realizations (about 16 realizations to compute the mean and about 128 realizations for the standard deviation) at least for the cytosolic calcium response. For other systems some trial may be involved. These results can be potentially used for deciding the number of realizations needed to compute meaningful statistics in stochastic simulations, at least for similar systems with a similar number of components.

VI. SUPPLEMENTARY MATERIAL

The supporting document "supplementary.pdf" contains additional text, Tables S1–3 and Fig. S1–4.[53]

NOMENCLATURE

CLE = chemical Langevin equation
CME = chemical master equation
IC = initial condition
KD = knockdown
ODE = ordinary differential equation
SHA = stochastic hybrid algorithm
SSA = stochastic simulation algorithm
H = the difference between the basal level of calcium response b and the peak level h
$K_j(\tau|\mathbf{X},t)$ = the number of times j-th reaction ($1 \leq j \leq M$) takes place during the time interval $[t, t+\tau]$
M = number of reactions
N = number of species
N_A = Avogadro's constant

M_f = number of fast reactions
M_s = number of slow reactions
N_r = number of realizations of simulations
$P\{a_j(\mathbf{X}),\tau\}$ = Poisson random variable whose mean and variance are $a_j\tau$
$P[\mathbf{X};t]$ = the probability of the system being in the state $\mathbf{X}$ at time t
$P_0[\tau|\mathbf{X},t]$ = the conditional probability that no reactions occur during the time interval $[t,t+\tau)$
V = fixed cellular volume
$\mathbf{X}(t)$ = state vector representing number of molecules of each species
$\mathbf{Y}(t)$ = continuous counterpart of $\mathbf{X}(t)$
Z_j = independent random variables on $(0,1)$
$a_j(\mathbf{X})$ = the propensity function of the jth reaction channel
c_j = the specific probability rate constant of the jth reaction
$h_j(\mathbf{X})$ = the number of possible combinations of reactants in the jth reaction
n_c = control parameter defining critical reactions
$p(\tau,j|\mathbf{X},t)$ = the probability that the next reaction will be the jth reaction and will occur during $[t+\tau,t+\tau+d\tau)$

Greek letters

α = control parameter deciding fast and slow reactions
β = control parameter deciding fast and slow reactions
$\mathcal{E}$ = normalized response difference
ν_j = vector whose entries are the numbers of molecules of each species added to or removed from the volume V due to the jth reaction
σ = standard deviation

$\tilde{\sigma}$ = normalized standard deviation
τ = time-interval

APPENDIX: EXISTING ALGORITHMS FOR STOCHASTIC SIMULATION

Three algorithms, namely, Gillespie algorithm, tau-leap method, and chemical Langevin equation, are reviewed. These algorithms are applied to a well-stirred biochemical system (molecules of each species are spread uniformly throughout a fixed control volume) at thermal equilibrium comprising M different chemical reactions and N different types of chemical species.

At any time t, the population of molecules within a fixed cellular volume V is uniquely described by a state vector $\mathbf{X}(t)$,

$$\mathbf{X}(t) = \{X_1(t), X_2(t), \ldots, X_N(t)\}^T, \tag{A1}$$

where $X_i(t)$ is the number of molecules of the ith species ($i=1,\ldots,N$). By definition, X_i are non-negative integers. The state vector $\mathbf{X}(t)$ changes whenever one of the M types of reactions occur.

Let $P[\mathbf{X};t]$ denote the probability of the system being in the state represented in Eq. (A1) at time t. Furthermore, let $a_j(\mathbf{X})$ denote the *propensity function* of the jth reaction channel, which is defined through $a_j(\mathbf{X})dt$, the probability that the jth reaction will occur during a (sufficiently small) time interval $[t,t+dt]$ given the system state $\mathbf{X}(t)$ at time t. The propensity function $a_j(\mathbf{X})$ can be expressed as[46]

$$a_j(\mathbf{X}) = c_j h_j(\mathbf{X}), \quad j \in \mathcal{M}, \quad \mathcal{M} = \{1,2,\ldots,M\}, \tag{A2a}$$

where $c_j > 0$ is the specific probability rate constant of the jth reaction and $h_j(\mathbf{X})$ is the number of possible combinations of reactants in the jth reaction. The former is given by

$$c_j = \begin{cases} k_j & \text{for monomolecular reactions} \\ \dfrac{2k_j}{N_A V} & \text{for bimolecular reactions with identical reactants} \\ \dfrac{k_j}{N_A V} & \text{for bimolecular reactions with different reactants,} \end{cases} \tag{A2b}$$

where $N_A = 6.022 \times 10^{23}$ mol^{-1} is Avogadro's constant and k_j is the macroscopic reaction rate constant.[56] The latter has the form

$$h_j(\mathbf{X}) = \begin{cases} 1 & \text{for reactions of type: } \phi \rightarrow \text{product(s) [no reactants]} \\ X_i & \text{for monomolecular reactions } [A \rightarrow B] \\ X_i(X_i-1)/2 & \text{for reactions with identical reactants } [A+A \rightarrow C] \\ X_i X_k & \text{for reactions with different reactants } [A+B \rightarrow C] \end{cases} \tag{A2c}$$

for some $1 \leq j \leq M$, and $1 \leq i,k \leq N$ with $i \neq k$.

Let the time-interval dt in the definition of $a_j(\mathbf{X})$ [Eq. (A2)] be small enough that at most one reaction occurs during $[t,t+dt)$, then $P[\mathbf{X};t]$ satisfies an ODE that is commonly called a chemical master equation (CME),[46]

$$\frac{dP[\mathbf{X};t]}{dt} = \sum_{j=1}^{M} \{a_j(\mathbf{X} - \boldsymbol{\nu}_j)P[\mathbf{X} - \boldsymbol{\nu}_j;t] - a_j(\mathbf{X})P[\mathbf{X};t]\},$$

(A3)

where $\boldsymbol{\nu}_j = (\nu_{j_1}, \ldots, \nu_{j_N})^T$ is a vector whose entries are the numbers of molecules of each species added to or removed from the volume V due to the jth reaction. For complex cellular processes, such as calcium dynamics in the signaling network described in Sec. III A, high-dimensionality of the CME [Eq. (A3)] renders its solutions computationally prohibitive. The standard simulation algorithms described below serve to overcome the computational burden associated with solving Eq. (A3).

1. Gillespie algorithm

Let $P_0[\tau|\mathbf{X},t]$ denote the conditional probability that no reactions occur during the time interval $[t,t+\tau)$ provided that the system is at state $\mathbf{X}$ at time t. Furthermore, let us assume that the reacting system is Markovian, i.e., the probability that no reactions occur during $[t,t+\tau+d\tau)$ equals the product of probability that no reactions occur during $[t,t+\tau)$ and probability that no reactions occur during $[t+\tau,t+\tau+d\tau)$. Then the definition of the propensity function implies that[46]

$$P_0[\tau+d\tau|\mathbf{X},t] = P_0[\tau|\mathbf{X},t][1 - a_{\text{sum}}(\mathbf{X})d\tau],$$

(A4)

$$a_{\text{sum}}(\mathbf{X}) \equiv \sum_{j=1}^{M} a_j(\mathbf{X}).$$

Taking the limit as $d\tau \to 0$ and solving the resulting ODE, we obtain

$$P_0(\tau|\mathbf{X},t) = e^{-a_{\text{sum}}(\mathbf{X})\tau}.$$

(A5)

Using the definition of P_0 and a_j, it can be shown[46] that the joint probability density function $p(\tau,j|\mathbf{x},t)$, which describes the probability that the next reaction will be the jth reaction and will occur during $[t+\tau,t+\tau+d\tau)$ given the present state of the system $\mathbf{X}(t)$, is given by $p(\tau,j|\mathbf{X},t)=P_0[\tau|\mathbf{X},t]a_j(\mathbf{X})$. Accounting for Eq. (A5), we obtain

$$p(\tau,j|\mathbf{X},t) = \frac{a_j(\mathbf{X})}{a_{sum}(\mathbf{X})} a_{sum}(\mathbf{X})e^{-a_{\text{sum}}(\mathbf{X})\tau}.$$

(A6)

The ratio $a_j(\mathbf{X})/a_{sum}(\mathbf{X})$ represents the density of a discrete random variable and serves to determine the next reaction. The remainder of the right-hand side of Eq. (A6), $a_{sum}(\mathbf{X})\exp[-a_{\text{sum}}(\mathbf{X})\tau]$ is the exponential density function of a continuous random variable, which corresponds to the time at which the next reaction will occur.

To advance the system from state $\mathbf{X}(t)$, the Gillespie algorithm generates two random variables r_1 and r_2 distrib-

uted uniformly on the unit interval $[0,1]$. According to Eq. (A6), a discrete random value j and continuous random value τ are selected as

$$\tau = \frac{1}{a_{\text{sum}}}\ln\left(\frac{1}{r_1}\right), \quad \sum_{j'=1}^{j-1} a_{j'} \leq r_2 a_{\text{sum}} \leq \sum_{j'=1}^{j} a_{j'}.$$

(A7)

The system is then updated according to $\mathbf{X}(t+\tau)=\mathbf{X}(t)+\boldsymbol{\nu}_j$.

A faster algorithm for exact stochastic simulation has been presented by Gibson and Bruck,[49] called "next reaction method," which can be used anywhere the Gillespie algorithm. This approach is about an order of magnitude faster than the Gillespie algorithm discussed above. However, this approach does not scale as well as the tau-leap algorithm discussed below as the number of molecules increases.

2. Tau-leap algorithm

The tau-leap algorithm[6] can be used to increase the computational efficiency of the Gillespie algorithm when it is used to simulate large reactive systems consisting of many reactions and molecules. This algorithm allows many reactions to take place simultaneously during a time interval $[t,t+\tau]$. Let $K_j(\tau|\mathbf{X},t)$ denote the number of times jth reaction $(1 \leq j \leq M)$ takes place during the time interval $[t,t+\tau)$, given the system state $\mathbf{X}(t)$ at time t. The value of τ is selected to satisfy the so-called "leap condition," which requires that none of the propensity functions a_j $(1 \leq j \leq M)$ suffers a noticeable change in its value. Then $K_j(\tau|\mathbf{X},t)$ can be approximated with a Poisson random variable $P\{a_j(\mathbf{X}),\tau\}$ whose mean and variance are $a_j\tau$. The system state is now updated according to

$$\mathbf{X}(t+\tau) = \mathbf{X}(t) + \sum_{j=1}^{M} \boldsymbol{\nu}_j P\{a_j(\mathbf{X}),\tau\}.$$

(A8)

As the time interval τ becomes smaller, it allows for few reactions to take place simultaneously, eventually reaching the limit of one reaction per τ. In this limit, $P\{a_j(\mathbf{x}),\tau\} \to 1$ and we get the Gillespie algorithm.

Algorithmic consistency requires that, in addition to satisfying the leap condition, τ be selected in a way that prevents number of any species from becoming negative. The binomial tau-leap algorithm[9,57] imposes this constraint by introducing a new control parameter n_c (typically a small positive integer), which defines "critical reactions" as those having at least one species with the number of molecules less than n_c. If there are one or more critical reactions then τ is chosen so that no critical reaction fires more than once. The binomial tau-leap algorithm[9,57] also expresses the leap condition in terms of a bound on the change rate of $a_j[\mathbf{X}(t)]$ as $|\Delta a_j(\mathbf{X}(t))| \leq \epsilon a_j(\mathbf{X}(t))$, where $0 < \epsilon \ll 1$.

3. Chemical Langevin equation

To increase the computational efficiency further, the leap time τ can be increased so that $a_j(\mathbf{X})\tau$ becomes large enough to ensure that it contains a large number of reactions for each reaction channel. Now the Poisson random variable $P\{a_j(\mathbf{X}),\tau\}$ can be approximated with a normal random variable[46] with the same mean and variance: $a_j[\mathbf{X}(t)]\tau$

$+\sqrt{a_j[\mathbf{X}(t)]\tau}Z_j$, where Z_j are independent normal random variables on the interval $(0,1)$. This approximation replaces Eq. (A8) with a CLE,

$$\mathbf{Y}(t+\tau) = \mathbf{Y}(t) + \tau\sum_{j=1}^{M}\boldsymbol{\nu}_j a_j[\mathbf{Y}(t)] + \sqrt{\tau}\sum_{j=1}^{M}\sqrt{\boldsymbol{\nu}_j a_j[\mathbf{Y}(t)]}Z_j,$$

(A9)

where $\mathbf{Y}(t)$ is a continuous counterpart of the discrete random variable $\mathbf{X}(t)$, replacing the number of molecules of the jth species, X_j, with the respective concentrations Y_j $(j = 1, \ldots, N)$.

[1] U. S. Bhalla, P. T. Ram, and R. Iyengar, Science **297**, 1018 (2002).
[2] B. Novak, J. J. Tyson, B. Gyorffy, and A. Csikasz-Nagy, Nat. Cell Biol. **9**, 724 (2007).
[3] M. R. Maurya and S. Subramaniam, Biophys. J. **93**, 709 (2007).
[4] U. Kummer, B. Krajnc, J. Pahle, A. K. Green, C. J. Dixon, and M. Marhl, Biophys. J. **89**, 1603 (2005).
[5] D. T. Gillespie, J. Phys. Chem. **81**, 2340 (1977).
[6] Y. Cao, D. T. Gillespie, and L. R. Petzold, J. Chem. Phys. **124**, 044109 (2006).
[7] V. Sotiropoulos, M. Contou-Carrere, P. Daoutidis, and Y. N. Kaznessis, IEEE/ACM Trans. Comput. Biol. Bioinf. **6**, 470 (2009).
[8] C. V. Rao and A. P. Arkin, J. Chem. Phys. **118**, 4999 (2003).
[9] A. Chatterjee, D. G. Vlachos, and M. A. Katsoulakis, J. Chem. Phys. **122**, 024112 (2005).
[10] X. Cai and J. Wen, J. Chem. Phys. **131**, 064108 (2009).
[11] M. W. Chevalier and H. El-Samad, J. Chem. Phys. **131**, 054102 (2009).
[12] H. Salis and Y. Kaznessis, J. Chem. Phys. **122**, 054103 (2005).
[13] D. Barik, M. R. Paul, W. T. Baumann, Y. Cao, and J. J. Tyson, Biophys. J. **95**, 3563 (2008).
[14] R. Ramaswamy and I. F. Sbalzarini, J. Chem. Phys. **132**, 044102 (2010).
[15] B. Mélykúti, K. Burrage, and K. C. Zygalakis, J. Chem. Phys. **132**, 164109 (2010).
[16] X. Cai, J. Chem. Phys. **126**, 124108 (2007).
[17] J. M. Frazier, Y. Chushak, and B. Foy, BMC Syst. Biol. **3**, 64 (2009).
[18] D. T. Gillespie, Y. Cao, K. R. Sanft, and L. R. Petzold, J. Chem. Phys. **130**, 064103 (2009).
[19] M. Rathinam, P. W. Sheppard, and M. Khammash, J. Chem. Phys. **132**, 034103 (2010).
[20] R. L. Karcher, J. T. Roland, F. Zappacosta, M. J. Huddleston, R. S. Annan, S. A. Carr, and V. I. Gelfand, Science **293**, 1317 (2001).
[21] K. Bedard, E. Szabo, M. Michalak, and M. Opas, Int. Rev. Cytol. **245**, 91 (2005).
[22] S. Johnson, M. Michalak, M. Opas, and P. Eggleton, Trends Cell Biol. **11**, 122 (2001).
[23] M. Michalak, P. Mariani, and M. Opas, Biochem. Cell Biol. **76**, 779 (1998).
[24] Y. Kim, J. S. Moon, K. S. Lee, S. Y. Park, J. Cheong, H. S. Kang, H. Y. Lee, and H. D. Kim, Biochem. Biophys. Res. Commun. **314**, 695 (2004).
[25] T. Hofer, L. Venance, and C. Giaume, J. Neurosci. **22**, 4850 (2002).
[26] J. Wagner and J. Keizer, Biophys. J. **67**, 447 (1994).
[27] G. Lemon, W. G. Gibson, and M. R. Bennett, J. Theor. Biol. **223**, 93 (2003).
[28] M. R. Maurya and S. Subramaniam, Biophys. J. **93**, 729 (2007).
[29] M. J. Berridge, M. D. Bootman, and H. L. Roderick, Nat. Rev. Mol. Cell Biol. **4**, 517 (2003).
[30] M. J. Berridge, J. Biol. Chem. **265**, 9583 (1990).
[31] T. Meyer and L. Stryer, Proc. Natl. Acad. Sci. U.S.A. **85**, 5051 (1988).
[32] E. G. Lakatta, T. M. Vinogradova, and V. A. Maltsev, Ann. N.Y. Acad. Sci. **1123**, 41 (2008).
[33] J. Mishra and U. S. Bhalla, Biophys. J. **83**, 1298 (2002).
[34] T. Doi, S. Kuroda, T. Michikawa, and M. Kawato, J. Neurosci. **25**, 950 (2005).
[35] J. L. Greenstein, R. Hinch, and R. L. Winslow, Biophys. J. **90**, 77 (2006).
[36] J. L. Greenstein and R. L. Winslow, Biophys. J. **83**, 2918 (2002).
[37] G. R. Van Den Brink, S. M. Bloemers, B. Van Den Blink, L. G. Tertoolen, S. J. Van Deventer, and M. P. Peppelenbosch, Microsc. Res. Tech. **46**, 418 (1999).
[38] T. F. Wiesner, B. C. Berk, and R. M. Nerem, Am. J. Physiol.: Cell Physiol. **39**, C1556 (1996).
[39] C. C. Fink, B. Slepchenko, I. Moraru, J. Watras, J. C. Schaff, and L. M. Loew, Biophys. J. **79**, 163 (2000).
[40] S. Rudiger, J. W. Shuai, W. Huisinga, C. Nagaiah, G. Warnecke, I. Parker, and M. Falcke, Biophys. J. **93**, 1847 (2007).
[41] M. S. Jafri, J. J. Rice, and R. L. Winslow, Biophys. J. **74**, 1149 (1998).
[42] M. Puceat and M. Jaconi, Cell Calcium **38**, 383 (2005).
[43] J. M. Raser and E. K. O'Shea, Science **309**, 2010 (2005).
[44] S. Schuster, M. Marhl, and T. Hofer, Eur. J. Biochem. **269**, 1333 (2002).
[45] Y. X. Li and J. Rinzel, J. Theor. Biol. **166**, 461 (1994).
[46] D. J. Higham, SIAM Rev. **50**, 347 (2008).
[47] E. L. Haseltine and J. B. Rawlings, J. Chem. Phys. **117**, 6959 (2002).
[48] E. L. Haseltine and J. B. Rawlings, J. Chem. Phys. **123**, 164115 (2005).
[49] M. A. Gibson and J. Bruck, J. Phys. Chem. A **104**, 1876 (2000).
[50] K. Vasudeva and U. S. Bhalla, Bioinformatics **20**, 78 (2004).
[51] U. S. Bhalla, Biophys. J. **87**, 733 (2004).
[52] G. W. DeYoung and J. Keizer, Proc. Natl. Acad. Sci. U.S.A. **89**, 9895 (1992).
[53] See supplementary material at http://dx.doi.org/10.1063/1.3496996 for additional text, Tables S1-3 and Fig. S1-4.
[54] E. A. Mastny, E. L. Haseltine, and J. B. Rawlings, J. Chem. Phys. **127**, 094106 (2007).
[55] G. Srinivasan, D. M. Tartakovsky, B. A. Robinson, and A. B. Aceves, Water Resour. Res. **43**, W12415 (2007).
[56] J. Goutsias, J. Chem. Phys. **122**, 184102 (2005).
[57] Y. Cao, D. T. Gillespie, and L. R. Petzold, J. Chem. Phys. **123**, 054104 (2005).